iScience

CellPress
OPEN ACCESS

Article

βig-h3-structured collagen alters macrophage phenotype and function in pancreatic cancer

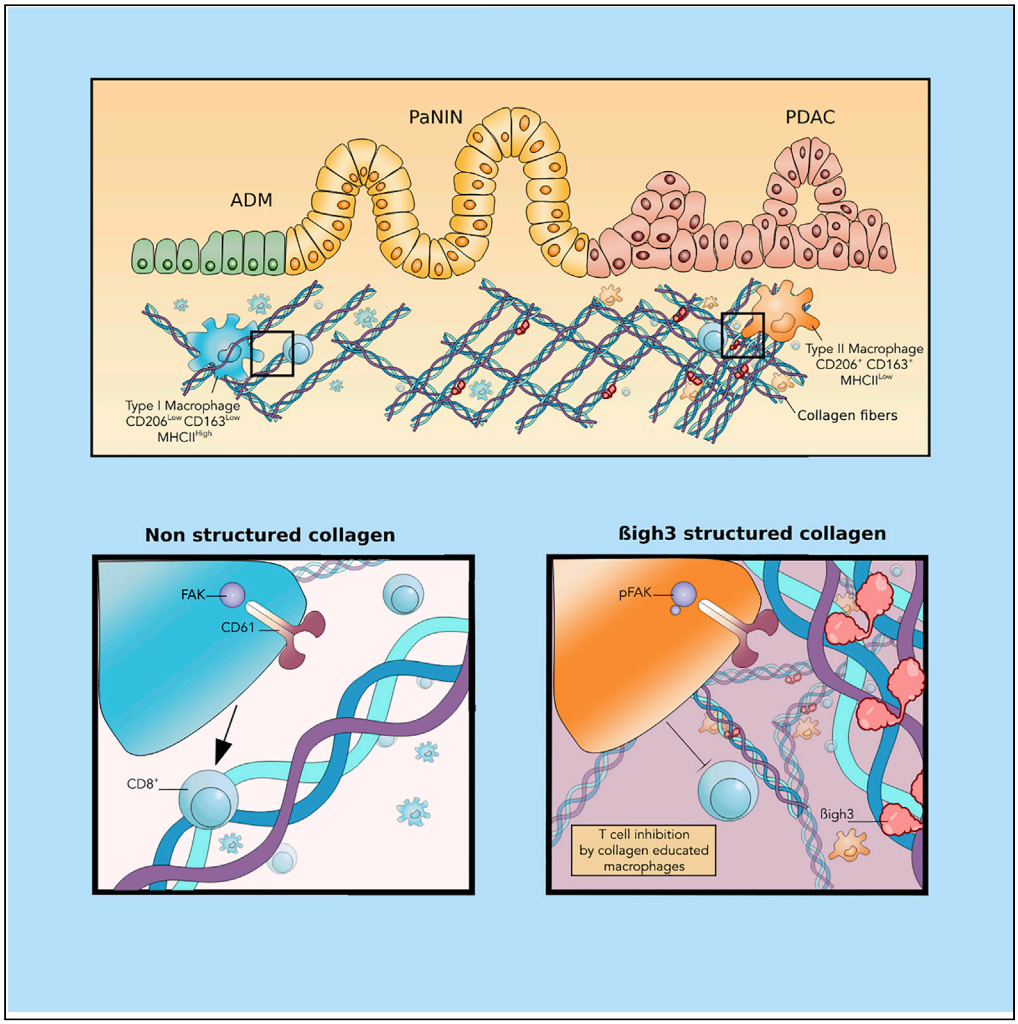

Sophie Bachy, Zhichong Wu, Pia Gamradt, Kevin Thierry, Pascale Milani, Julien Chlasta, Ana Hennino

ana.hennino@inserm.fr

Highlights

Atomic force microscopy of βig-h3-structured collagen

In vitro and *in vivo* macrophage education on structured collagen

In vitro macrophage phenotype imprinting is stable *in vivo*

Bachy et al., iScience *25*, 103758
February 18, 2022
https://doi.org/10.1016/j.isci.2022.103758

iScience

CellPress
OPEN ACCESS

Article

βig-h3-structured collagen alters macrophage phenotype and function in pancreatic cancer

Sophie Bachy,[1,2,3,5] Zhichong Wu,[1,2,3,5] Pia Gamradt,[1,2,3] Kevin Thierry,[1,2,3] Pascale Milani,[4] Julien Chlasta,[4] and Ana Hennino[1,2,3,6,*]

SUMMARY

Macrophages play an important role in immune and matrix regulation during pancreatic adenocarcinoma (PDAC). Collagen deposition massively contributes to the physical and functional changes of the tissue during pathogenesis. We investigated the impact of thick collagen fibers on the phenotype and function of macrophages. We recently demonstrated that the extracellular protein βig-h3/TGFβi (Transforming growth factor-β-induced protein) plays an important role in modulating the stiffness of the pancreatic stroma. By using atomic force microscopy, we show that βig-h3 binds to type I collagen and establishes thicker fibers. Macrophages cultured on βig-h3-structured collagen layers display a different morphology and a pro-tumoral M2 phenotype and function compared to those cultured on non-structured collagen layers. *In vivo* injection of those instructed CD206^{+}CD163^{+} macrophages was able to suppress T cell responses. These results reveal for the first time that the collagen structure impacts the phenotype and function of macrophages by potentiating their immunosuppressive features.

INTRODUCTION

We have recently demonstrated that the extracellular matrix protein βig-h3/TGFβi (Transforming growth factor-β-induced protein) plays an important role in modulating the stiffness of tumor microenvironment (TME) in pancreatic adenocarcinoma (PDAC) (Goehrig et al., 2019). Previous studies established that βig-h3 binds to type I, II, and IV collagens as well as to biglycan and decorin thereby influencing cell-to-cell, cell-to-collagen, and cell-to-matrix interactions (Bae et al., 2002; Hashimoto et al., 1997). The *tgfbi* gene encodes a 683-amino acid protein that contains a secretory signal sequence, an N-terminal cysteine-rich EMI domain, four fasciclin 1 domains, and an RGD (Arg–Gly–Asp) motif (Skonier et al., 1992, 1994).

Though the pancreas is a soft tissue at homeostasis, collagen deposition massively contributes to the "physical and functional" changes of the tissue that occur during pathogenesis. This process results in a stiffened pancreatic parenchyma and represents a significant risk factor for developing PDAC (Laklai et al., 2016). Because collagen fibers adjacent to pancreatic lesions are significantly thicker in patients with the shortest survival, we investigated the impact of thick collagen fibers on the phenotype and function of macrophages during PDAC. We previously showed that, aside from its role in modulating collagen stiffness, βig-h3 has immunosuppressive properties hampering T cell activation and is able to reprogram macrophages (Goehrig et al., 2019; Patry et al., 2015). It is well-known that macrophages play an important role in the immune responses in pancreatic fibrosis, a risk factor for PDAC, and we thus speculated that βig-h3 may affect macrophage properties by modulating collagen fibers.

RESULTS

Matrix protein βig-h3 structures collagen I in thicker fibers

We first investigated the localization of βig-h3 and collagen I by performing immunofluorescence (IF) microscopy on pancreatic samples obtained from the *p48-Cre*, *Kras^{G12D}* (KC) mouse model, which develops pancreatic intraepithelial neoplasias (PanINs) from the age of 1.5 months old (Hingorani et al., 2003). As shown in Figure 1A, we observed that both proteins co-localized around pancreatic neoplastic lesions. Moreover, F4/80^{+} macrophages were localized in close proximity to βig-h3 around PanIN lesions

[1]Cancer Research Center of Lyon, UMR INSERM1052, CNRS5286, 69373 Lyon, France

[2]Université Lyon 1, 69000 Lyon, France

[3]Centre Léon Bérard, 69008 Lyon, France

[4]Biomeca, 69007 Lyon, France

[5]These authors contributed equally

[6]Lead contact

*Correspondence: ana.hennino@inserm.fr

https://doi.org/10.1016/j.isci.2022.103758

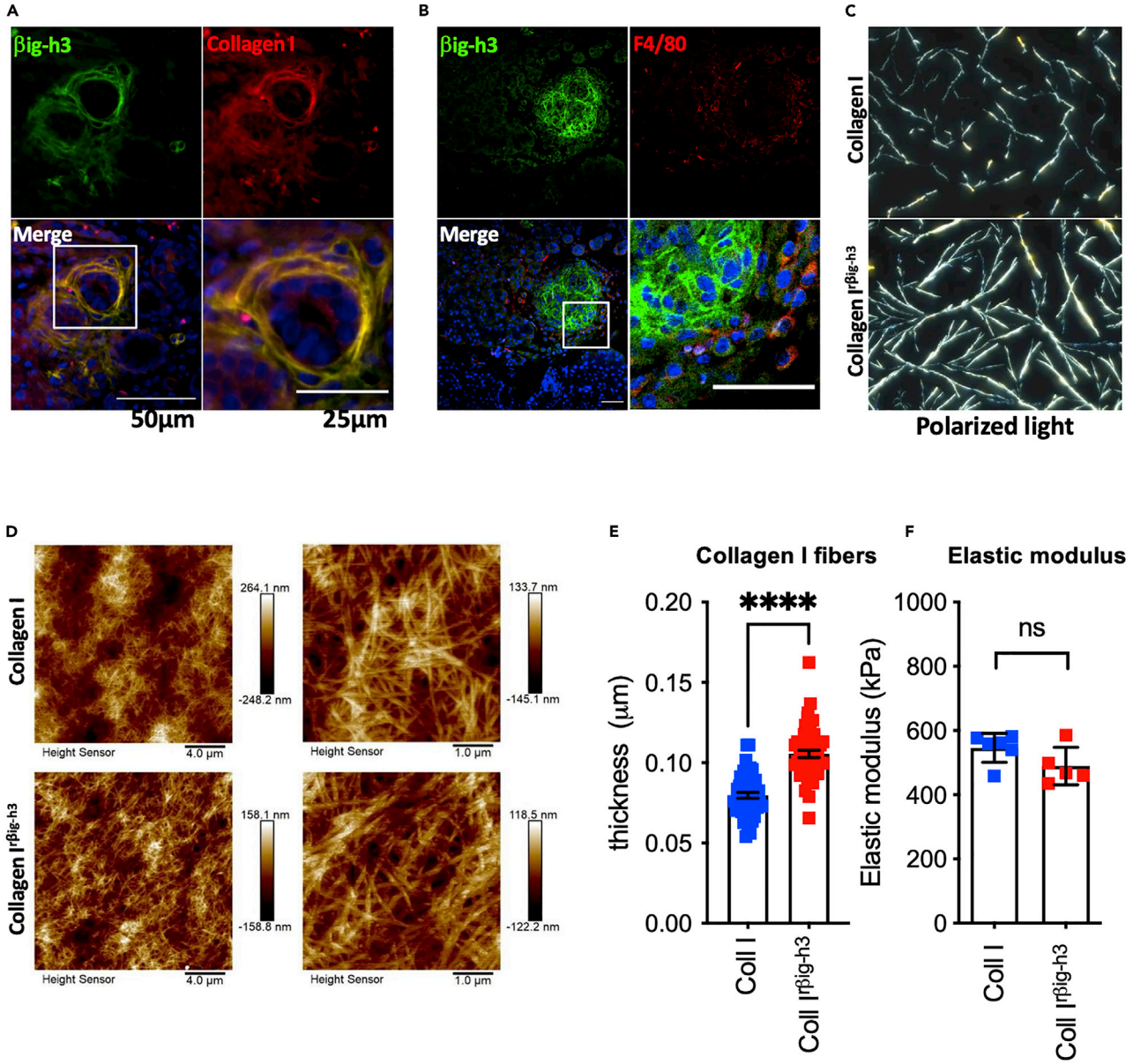

Figure 1. rβig-h3 structures collagen I into thick fibers

(A and B): Representative micrographs of immunofluorescence staining in pancreata from three-months-old KC mice for (A) βig-h3 (green), collagen I (red) or (B) βig-h3 (green) and F4/80 (red); (A, B) nuclear counterstaining in DAPI (blue).

(C) Representative micrographs taken with polarized light of collagen I structured in the absence (top) or presence (bottom) of rβig-h3 and stained with Sirius Red.

(D) Thickness topography measured by AFM of representative regions of collagen I structured in the absence (up) or presence (bottom) of rβig-h3. Two different magnifications are shown.

(E) Quantification of collagen I fiber thickness measured by AFM.

(F) Quantification of the Elastic modulus measured by AFM. Student's t-test ****p< 0.0001, ns - not significant. Error bars 50 µm, 25 µm.

(Figure 1B). A previous study having shown that βig-h3 was able to interact with collagen (Hashimoto et al., 1997), we generated collagen I matrices in the presence or absence of human recombinant βig-h3 (rβig-h3). Analysis of Sirius Red-stained collagen I matrices under polarized light allowed us to evaluate the effect of rβig-h3 on their microarchitecture (Figure 1C). In the presence of rβig-h3, the structure of the collagen I matrices developed into a network with higher density with thicker collagen fibers. In order to confirm these results, we performed quantitative topological analysis by atomic force microscopy which revealed that the

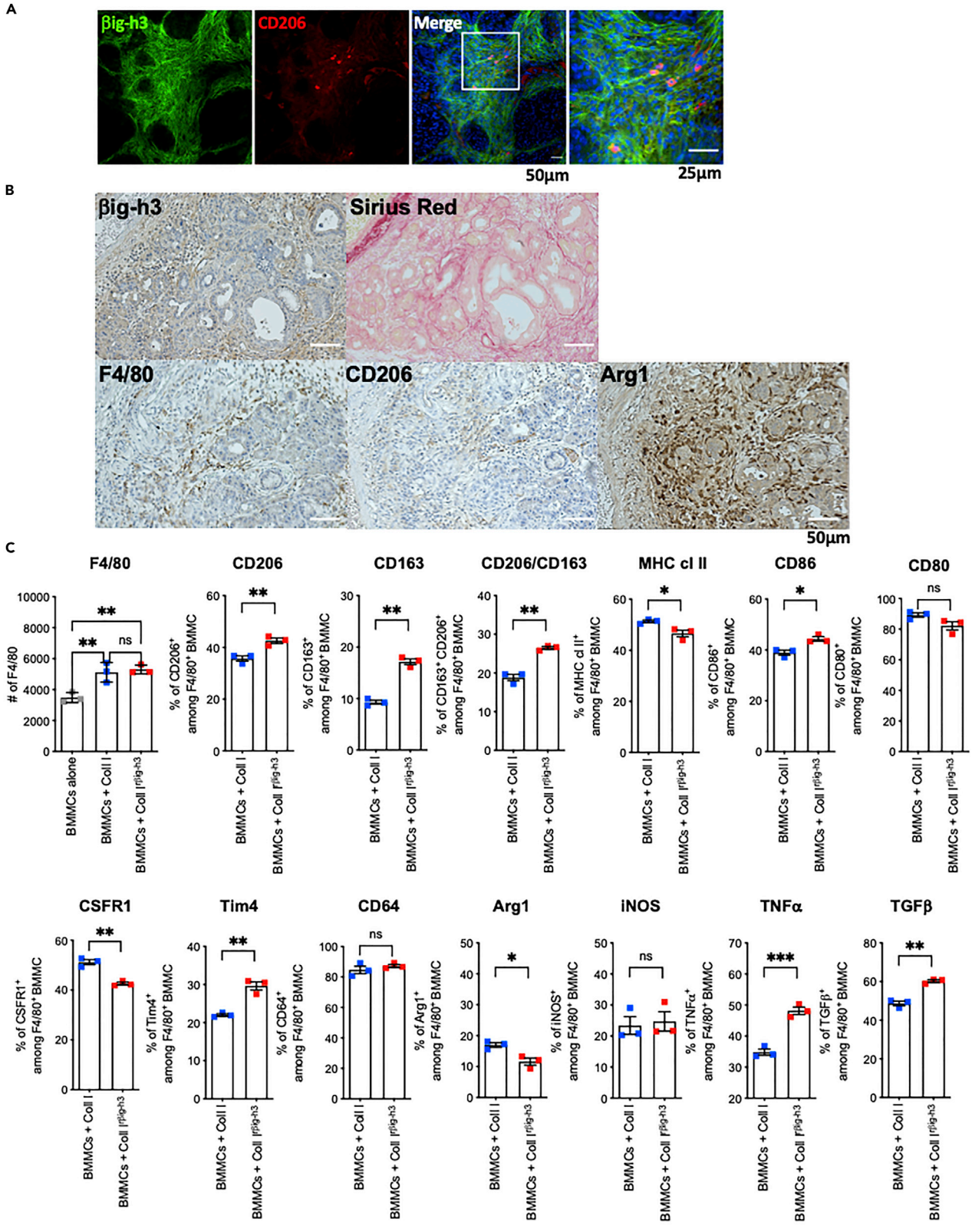
A
βig-h3
CD206
Merge
50μm
25μm
B
βig-h3
Sirius Red
F4/80
CD206
Arg1
50μm
C
F4/80
CD206
CD163
CD206/CD163
MHC cl II
CD86
CD80
# of F4/80
% of CD206+ among F4/80+ BMMC
% of CD163+ among F4/80+ BMMC
% of CD163+ CD206+ among F4/80+ BMMC
% of MHC cl II+ among F4/80+ BMMC
% of CD86+ among F4/80+ BMMC
% of CD80+ among F4/80+ BMMC
BMMCs alone
BMMCs + Coll I
BMMCs + Coll Iβig-h3
ns
CSFR1
Tim4
CD64
Arg1
iNOS
TNFα
TGFβ
% of CSFR1+ among F4/80+ BMMC
% of Tim4+ among F4/80+ BMMC
% of CD64+ among F4/80+ BMMC
% of Arg1+ among F4/80+ BMMC
% of iNOS+ among F4/80+ BMMC
% of TNFα+ among F4/80+ BMMC
% of TGFβ+ among F4/80+ BMMC

Figure 2. rβig-h3-structured collagen I fibers modulate the phenotype and function of macrophages

(A) Representative photographs of immunofluorescence staining of pancreata from three-months-old KC mice stained for βig-h3 (green) and CD206 (red). Nuclear counterstaining in DAPI (blue).

(B) Representative photographs of βig-h3, F4/80, CD206, and Arg1 staining on serial section of pancreata from three-months-old KC mice.

(C) FACS analysis of BMMCs cultured alone or on collagen I structured in the absence (BMMCs + Col I) or presence of rβig-h3 (BMMCs + Col $I^{r\beta ig\text{-}h3}$). Representative data of three independent experiments with three in vitro replicates per group are shown. *p<0.05, **p<0.01. Error bars 50 μm, 25 μm.

diameter of collagen fibers had increased in the presence of rβig-h3 (Figure 1E) whereas the elastic modulus measurements were similar in both conditions (Figure 1F). These results show that βig-h3 plays a role in structuring collagen I during fibrillogenesis.

rβig-h3-structured collagen I fibers modulate the phenotype and function of macrophages

Having detected the presence of macrophages in close proximity to PanIN lesions in mouse pancreatic cancer, we sought to determine the phenotype of macrophages in contact with endogenous βig-h3 within these tissues. We observed that macrophages in close contact with βig-h3 were positive for CD206 (Figure 2A), a well described marker associated with an M2 phenotype. To further characterize the phenotype of these macrophages *in situ*, we performed immunohistochemistry on serial sections of pancreatic tumors from KC mice stained for βig-h3, F4/80, CD206, and Arg1 as well as Sirius Red. We thereby confirmed M2 phenotype of $F4/80^+$ macrophages in close proximity to βig-h3 and collagen I, as they co-expressed CD206 and Arg1 (Figure 2B).

Next, we attempted to determine the direct effect of βig-h3-structered collagen fibers on the phenotype and function of macrophages. To achieve this, we cultured bone marrow-derived mononuclear cells (BMMCs) for 48 h on collagen I matrices generated in the presence or absence of rβig-h3. Flow cytometric analysis of recovered BMMCs revealed that rβig-h3-structured collagen I decreased MHC cl II and CSFR1 expression but increased CD206, CD163, CD86, and Tim4 surface expression (Figure 2C). The expression of CD80 and CD64 was similar in both conditions. We detected a small but significant decrease in Arg1 in the presence of rβig-h3-structured collagen I. We further detected increased TNFα and TGFβ cytokine production. Overall, these results indicate that βig-h3-structured collagen I in the TME might promote a pro-tumorigenic macrophage phenotype, displaying an M2 signature associated with increased CD206 and CD163 surface expression as well as augmented TGFβ cytokine production.

rβig-h3-structured collagen I fibers activate FAK signaling pathway in macrophages

Because the thickness of the collagen fibers was increased in the presence of βig-h3, we next investigated whether culturing BMMCs on collagen I structured in the absence or presence of rβig-h3 would have any impact on the cellular morphology. Morphological analysis of BMMCs revealed more spherical macrophages with fewer processes when cultured for 48 h on rβig-h3-structured collagen I compared to those on non-structured collagen I after 48 h of culture (Figures 3A and 3B). We then performed western blot analysis of FAK, phosphorylated FAK (pFAK) on macrophages cultured on plastic or on structured collagen I in the absence or presence of rβig-h3 for 48 h. BMMCs cultured on rβig-h3-structured collagen I displayed a greater increase in pFAK compared to non-structured collagen I (Figure 3C). These results indicate that rβig-h3-structured collagen I is able to not only modulate the cellular morphology of the cells but also induce FAK phosphorylation and hence its stronger activation in this condition. To verify whether the FAK phosphorylation mediated the change in the BMMC morphology, we added the pFAK inhibitor (Y15) to cell cultures. This restored the morphology of macrophages grown on rβig-h3-structured collagen I that resembled to those grown on non-structured collagen I (Figures 3D–3F). Furthermore, we evaluated their phenotype by flow cytometric analysis and revealed that pFAK treatment downregulated the CD163 and CD206 expression (Figure 3G). Altogether, these results suggest that rβig-h3-structured collagen I modulates the morphology of macrophages and subsequently their phenotype and function.

rβig-h3-structured collagen I promotes an immunosuppressive macrophage phenotype

Having established that culturing BMMCs on collagen I structured in the absence or presence of rβig-h3 affected the functional and morphological phenotype, we next evaluated its effect on T cell activation. We co-cultured $CD8^+$ T cells with BMMCs generated on plastic on collagen I or rβig-h3-structured collagen I at indicated ratios (4:1 or 2:1 or 1:1) and determined their proliferation by CFSE dilution as well as their activation based on the surface expression of CD69 and CD44. Whereas CSFE dilution revealed four to five cell divisions of $CD8^+$ T cells co-cultured with BMMCs generated on plastic or non-structured collagen

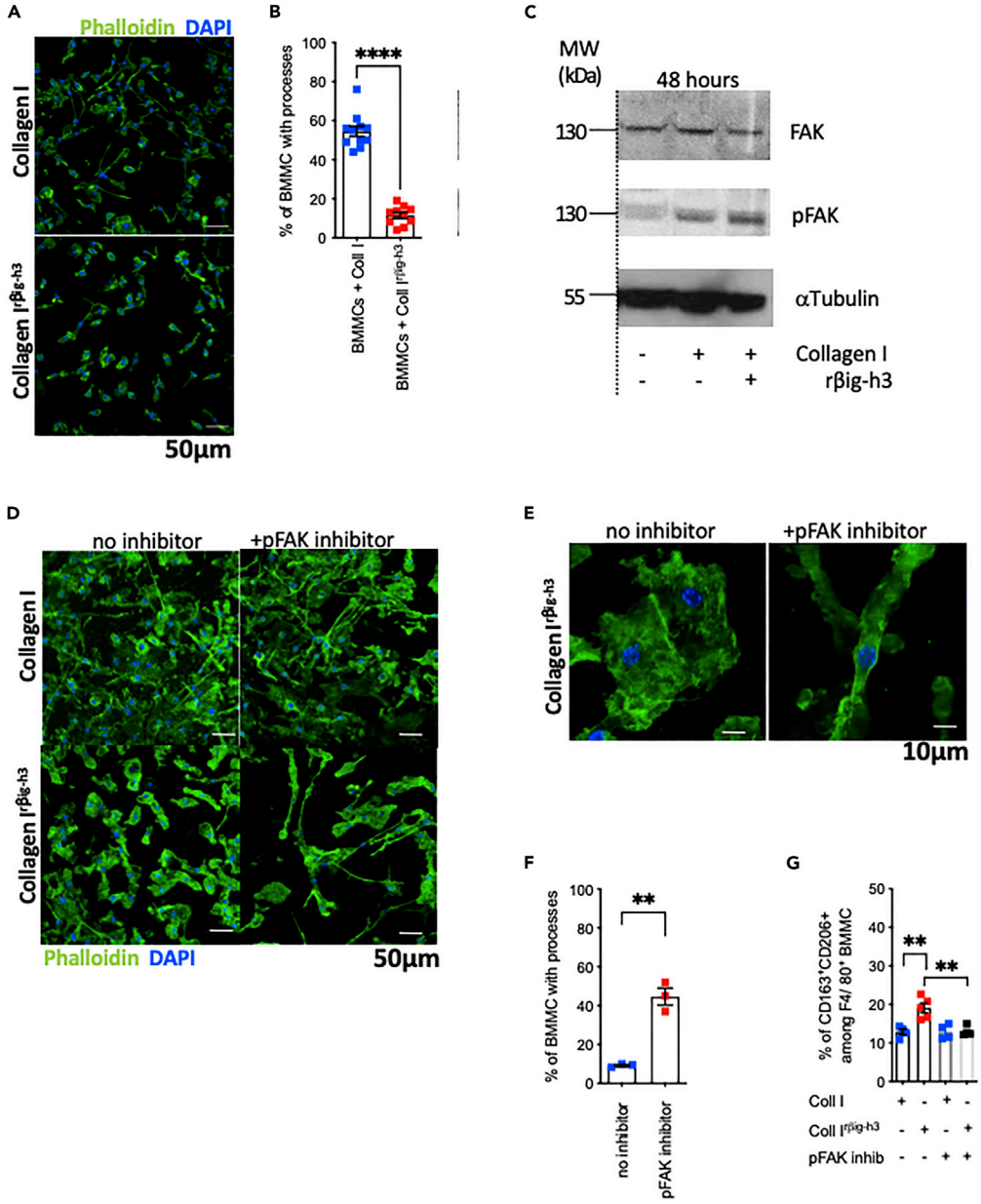

Figure 3. rβig-h3-structured collagen I fibers activate the FAK signaling pathway in macrophages

(A) Representative photographs of phalloidin immunofluorescence staining of BMMCs cultured on collagen I structured in the absence (left) or presence (right) of rβig-h3.

(B). Quantification of the processes of BMMCs cultured on collagen I structured in the absence or presence of rβig-h3.

(C) Western blot analysis of FAK, pFAK, and tubulin of BMMCs cultured on plastic, collagen I, or βig-h3-structured collagen I.

(D) Representative micrographs of phalloidin immunofluorescence staining of BMMCs cultured on collagen I structured in the absence (up) or presence (down) of rβig-h3 and with (left) or without (right) Y15.

(E) High-magnification micrographs of BMMCs cultured on rβig-h3-structured collagen in the absence (left) or presence (right) of Y15 inhibitor.

(F) Quantification of the processes detected in E. Each point represents an individual in vitro replicate.

(G) FACS analysis of % of $CD163^{+}CD206^{+}$ cells among F4/80+ BMMCs cultured on collagen I structured in the absence (BMMCs + Col I) or presence of rβig-h3 (BMMCs + Col $I^{rβig\text{-}h3}$) in absence or presence of pFAK inhibitor. Representative data of two independent experiments with five replicates per condition are shown. **p< 0.01, ****p< 0.0001. Error bars 50 µm, 25 µm.

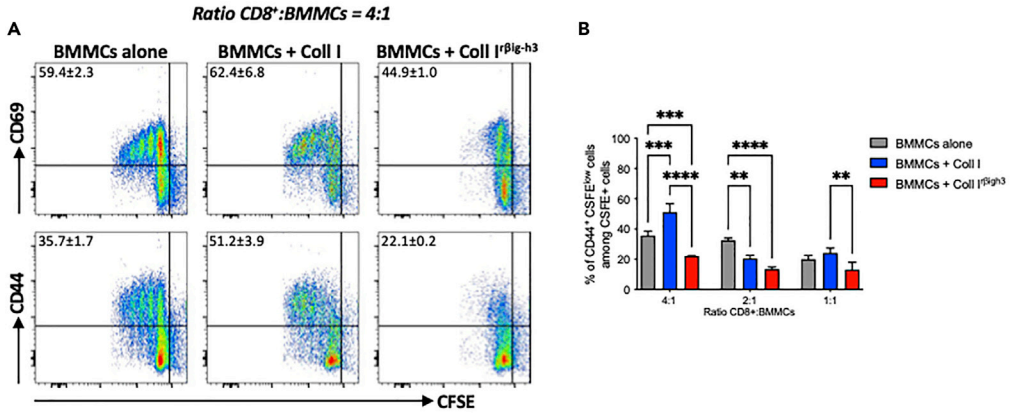

Figure 4. rβig-h3-structured collagen I fibers instruct macrophages with immunosuppresive properties

(A) Representative dot plots of CFSE and CD69 or CFSE and CD44 staining of CD8+T cells that have been cultured with BMMCs (ration CD8:BMMC 4:1) grown on plastic (BMMC alone), collagen I (BMMC+ coll I), or on βig-h3-structured collagen I (BMMC+ Coll I$^{rβig\text{-}h3}$).

(B) Quantification of the proliferating CD44$^+$ CD8$^+$ T in different ratios (4:1, 2:1, and 1:1). Representative of two independent experiments with three in vitro replicates per group. **p<0.01, ***p< 0.001, and ****p< 0.0001.

I, CD8$^+$ T cell proliferation was arrested after two divisions when co-cultured with BMMCs generated on rβig-h3-structured collagen I (Figure 4A). CD44 and CD69 expression of CD8$^+$ T cells was also significantly reduced when they were co-cultured with BMMCs generated on rβig-h3-structured collagen I confirming their immunosuppressive capacity (Figures 4A and 4B). In addition, this immunosuppressive effect of educated BMMC was dependent on the contact with CD8$^+$ T cells, because the use of condition media generated from different condition (plastic, on collagen I or rβig-h3-structured collagen I) displayed limited impact in CD8$^+$ T cell activation (Figure S1).

βig-h3-structured collagen I educated macrophages are immunosuppressive *in vivo*

In order to determine whether the structuration of collagen I in the absence or presence of rβig-h3 affects recruitment and phenotype of macrophages *in vivo*, we subcutaneously injected the GFP-tagged primary KIC (GFP$^+$ KIC) tumor cell line, which was generated from the pancreas of GEMM mice as previously described (Goehrig et al., 2019), embedded in non-structured or rβig-h3-structured collagen I into the flanks of Rag2KO mice. Five days after the injection, we evaluated the phenotype of recruited macrophages (Figure 5A). As shown in Figure S2, the non-structured collagen I and rβig-h3-structured collagen I were still detected in the subcutaneous plugs at day 5. We show that although less F4/80$^+$ macrophages were recruited when tumor cells were embedded in rβig-h3-structured collagen I (Figure 5B), the macrophages displayed increased CD206 expression as well as increased production of TGF-β and TNF-α cytokines suggesting an M2 phenotype (Figure 5B).

In order to investigate if the phenotype acquired by the macrophages was stable, we performed subcutaneously injection of C57BL/6 (WT) mice with GFP$^+$ KIC tumor cells and BMMCs generated on plastic, collagen I, or rβig-h3-structured collagen I. Five days later, we evaluated the number of tumor cells within the graft and the BMMC phenotype (Figure 6A). While the co-injection of BMMCs generated on plastic and non-structured collagen I resulted in equivalent number of tumor cells, this number was significantly increased, when GFP$^+$ KIC cells were co-injected with BMMCs generated on rβig-h3-structured collagen 1 (Figure 6B). Moreover, FACS analysis revealed that after the co-injection of BMMCs generated on rβig-h3-structured collagen I, the number of F4/80$^+$ BMMC was higher suggesting a better survival *in vivo*. In addition, these BMMCs were conserving CD206 expression and acquired CD163. These results indicate that education of BMMC on βig-h3-structured collagen I results in a stable phenotype that is preserved after *in vivo* injection.

βig-h3 depletion reprograms M2 macrophages phenotype *in vivo*

In order to determine if the modulation of βig-h3 *in vivo* affects the macrophage phenotype, WT mice were subcutaneously injected with GFP$^+$ KIC tumor cells. Starting from day 10, the mice were treated

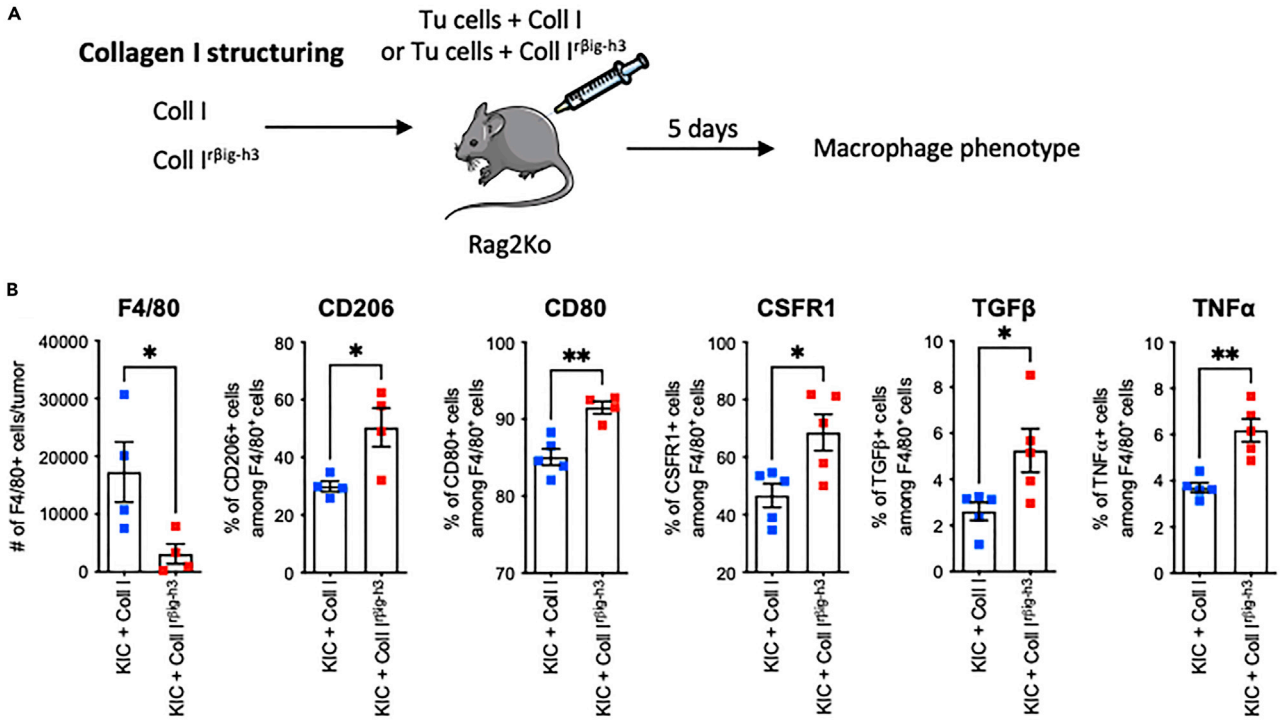

Figure 5. rβig-h3-structured collagen I fibers are able to instruct immunosuppressive macrophage phenotype in vivo

(A) Experimental setting.

(B) FACS analysis of the percentages of F4/80$^+$CD45$^+$, CD206$^+$F4/80$^+$, CD80$^+$F4/80$^+$, CSFR1$^+$F4/80$^+$, TGFβ$^+$F4/80$^+$, and TNFα$^+$F4/80$^+$ cells collected in A. *p<0.05, **p<0.01. Representative of two independent experiments with five mice per group.

with anti-βig-h3 monoclonal Ab (clone 18B3) twice a week for two weeks. At day 24, the mice were sacrificed, the tumor weight was evaluated, and flow cytometry analysis was performed in order to establish the impact on macrophages phenotype (Figure 7A). We evaluated the efficiency of the anti-βig-h3 mAb treatment by IHC staining of the tumor graft and shown decreased βig-h3 staining in the treated condition compared to control IgG1 Ab (FigureS3A). We show that mice treated with anti-βig-h3 exhibit diminished tumor weight compared to control IgG1 Ab-treated mice (Figure 7B). Furthermore, FACS analysis showed similar recruitment of CD45$^+$ total hematopoietic cells as well as F4/80 macrophages in the two conditions (Figures 7C and 7D). More importantly, the recruited macrophages express less CD206 and Arg1 (Figures 7E and 7F), suggesting a diminished M2 phenotype in the absence of βig-h3. Furthermore, we detected more CD8$^+$ cells that present a non-exhausted phenotype associated with reduced PD-1 expression (Figures S3B and S3C).

DISCUSSION

We report here for the first time that the matrix protein βig-h3 is able to structure collagen I into thicker fibers. These fibers are able to induce changes in morphology of macrophages that are accompanied by FAK phosphorylation. More importantly, we showed that these fibers skew the polarization of the macrophages toward an M2 phenotype associated with CD206 expression and MHC cl II and CSFR1 downregulation. Furthermore, these M2 macrophages acquired an immunosuppressive phenotype because they were able to reduce CD8$^+$ T cells proliferation and activation upon co-culture *in vitro*. This phenotype is stable *in vivo* because the injection of those macrophages led to increased number of tumor cells and to the maintenance of CD206 expression and acquisition of CD163 marker.

Tumor-associated macrophages are one of the most abundant immune cell populations in the TME representing up to 50% of all CD45$^+$ cells (Diskin et al., 2020). Macrophages represent a plastic cell population that can be polarized into several phenotypes depending on the cytokine environment. On one hand, there are M1 macrophages that are associated with Th1 responses, high phagocytic activity, and inflammatory cytokine secretion. On the other hand, there are M2 macrophages associated with Th2 responses,

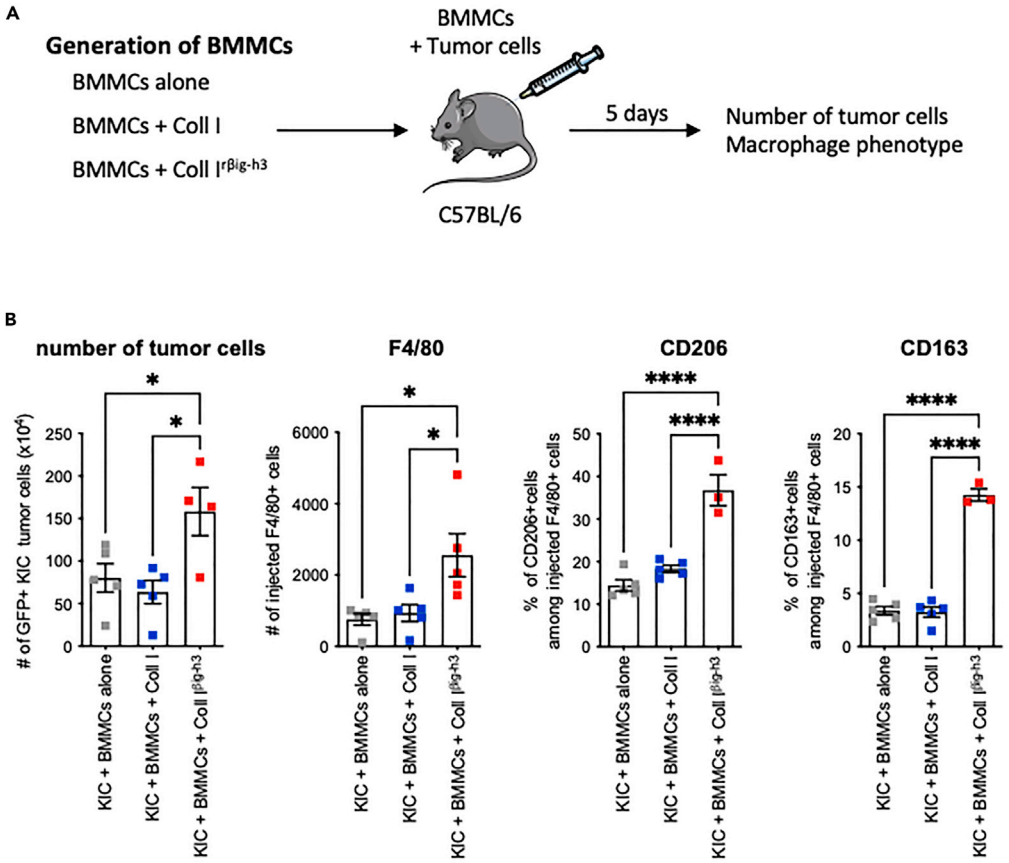

Figure 6. rβig-h3-structured collagen I educated macrophages maintain their phenotype after in vivo injection

(A and B) Experimental setting (B) FACS analysis of the number of tumor cells (GFP tagged), and the percentages of F4/80$^+$CD45$^+$, CD206$^+$F4/80$^+$, and CD163$^+$F4/80$^+$. *p<0.05, ****p< 0.0001.Representative of two independent experiments with five mice per group.

extracellular matrix remodeling, and immunosuppressive cytokine secretion (Mantovani et al., 2004). In PDAC, tumor-associated macrophages are associated with a lower overall survival and fibrosis in both preclinical mouse models and patients (Hu et al., 2016; Zhu et al., 2017). In addition, they have been shown to promote tumor growth by different mechanisms such as epithelial to mesenchymal transition of tumor cells (Liu et al., 2013), secretion of immunosuppressive cues (TGFβ, CCL22, CCL2, and CCL18), and, more generally, the re-shaping of the TME due to M2 functions. In the present study, we initially demonstrated that βig-h3-structured collagen plays an important role in educating macrophages toward an M2 phenotype. We show that this phenotype is associated with a morphological change from an originally spindle shape toward a more spherical appearance with reduced processes. Of note, other studies characterized M2 macrophages as elongated rather than spherical (Ruiz-Valdepenas et al., 2011), which seems to contrast with our data. We hypothesize that the acquisition of an M2 phenotype was previously achieved by adding soluble factors (*i. e.* Interleukin-4 and -13) to the differentiation medium, which differs from our own experimental approach based on substrate "education" through different collagen matrices structured in the absence or presence of rβig-h3. In our setting, rβig-h3-structured collagen I increased FAK phosphorylation and thereby augmented the adhesion points to the substrate facilitating a spherical shape with higher surface contact. Furthermore, the acquired phenotype was conserved after *in vivo* injection indicating that *in vitro* education induced a highly stable macrophage signature.

Aside from macrophages, the critical role of CD8$^+$ T cells in tumor clearance is undisputed. CD8$^+$ T cell tumor infiltration is thought to reflect a good prognosis (Galon et al., 2006). Our findings suggest that βig-h3-structured collagen I educated macrophages play an important immunosuppressive role because they inhibited the CD8$^+$ T cell proliferation *in vitro*. We show that these macrophages induced a CD8$^+$

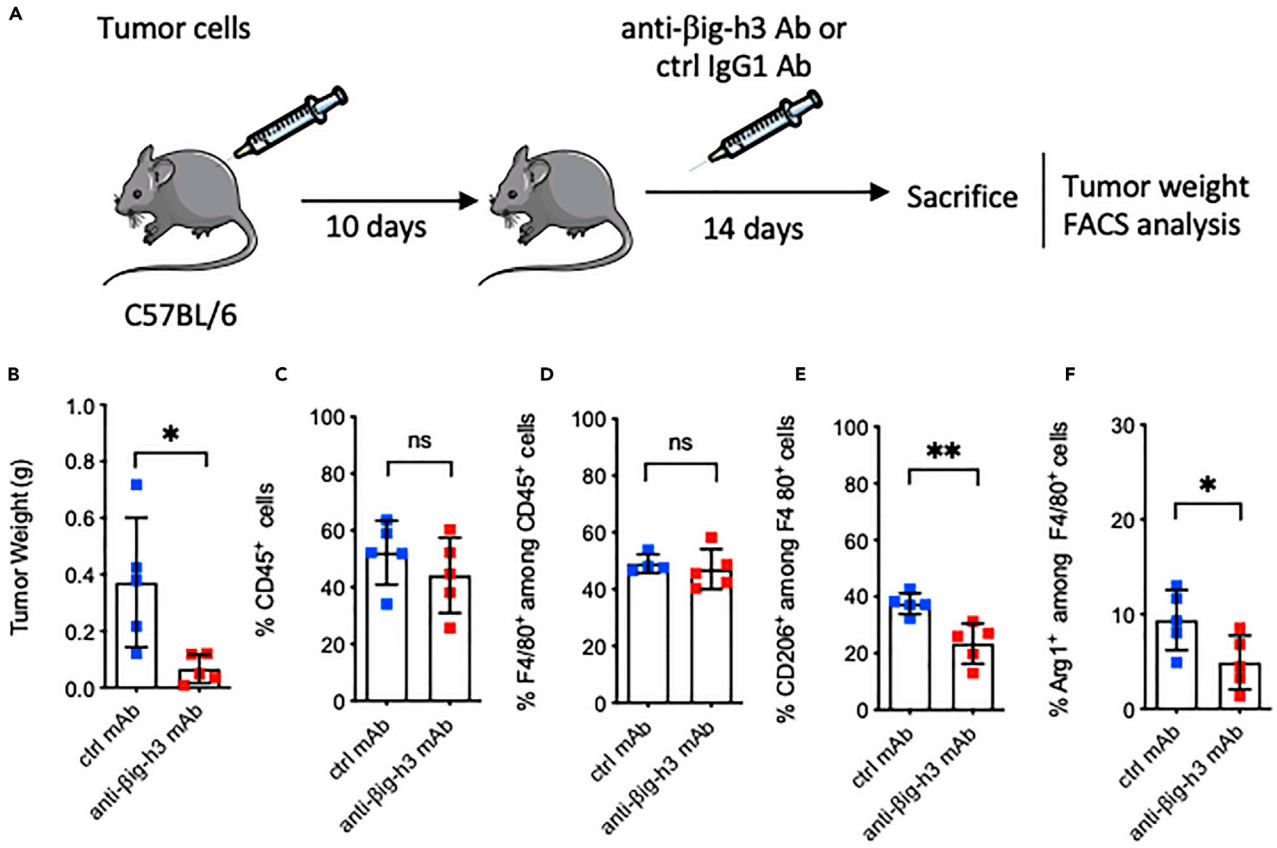

Figure 7. βig-h3 Ab depletion in vivo reprograms macrophage phenotype in the tumor microenvironment

(A) Experimental setting.

(B) Tumor weight of mice treated in A.

(C-F) FACS analysis of the percentages of $CD45^+$ (C), $F4/80^+CD45^+$(D), $CD206^+F4/80^+$(E), and $Arg1^+F4/80^+$ (F) cells collected in A. *p<0.05, **p<0.01. Representative of two independent experiments with fivemice per group.

T cell proliferation arrest accompanied with reduced expression of well-known activation markers such as CD69 and CD44. Previous findings demonstrated that bone marrow grown in a high-density collagen matrix compared with a low-density collagen matrix had higher immunosuppressive capacities inhibiting the proliferation of $CD8^+$ T cell *in vitro* (Kuczek et al., 2019; Larsen et al., 2020). Our findings highlight a new dimension of collagen organization in addition to matrix density structured in the presence of other extracellular matrix molecules, namely βig-h3 resulting in an immunosuppressive macrophage phenotype.

Furthermore, we revealed that this "M2 education" of macrophages can occur *in vivo* upon injection of tumor cells embedded in βig-h3-structured collagen because recruited macrophages also displayed an immunosuppressive phenotype.

This phenotype imprinted *in vitro* the macrophage phenotype imprinted *in vitro* by the βig-h3-structured collagen was highly stable, as "M2 characteristics" were maintained even after injection *in vivo* in combination with tumoral cells. Our results provide the first demonstration that the architecture of stromal collagen has a significant impact on the outcome of anti-tumoral immune responses because it alters the phenotype of macrophages toward a sustained M2 phenotype with immunosuppressive properties. These physical and functional modifications of the collagen in the context of pancreatic cancer might lead to the "reprogramming" of the TME by instructing $F4/80^+$ macrophages to become immunosuppressive. Importantly, our findings also show that *in vivo* depletion of the βig-h3 protein by a mAb approach diminishes the M2 phenotype macrophages. Further investigations should address how to disrupt βig-h3 binding to collagen, as this may lead to macrophages reprogramming in the pancreatic cancer TME with a potential therapeutic effect.

STAR★METHODS

Detailed methods are provided in the online version of this paper and include the following:

- KEY RESOURCES TABLE
- RESOURCE AVAILABILITY
  - Lead contact
  - Materials availability
  - Data availability
- METHOD DETAILS
  - Mice
  - Generation of collagen matrices
  - BMMC generation and education
  - KIC tumor cell line
  - Atomic force microscopy measurements and collagen fibrils analysis
  - Immunofluorescence staining
  - Confocal microscopy
  - Western blot
  - FACS analysis
  - T cell activation assay
  - Short term tumor implantation assay
- QUANTIFICATION AND STATISTICAL ANALYSIS

SUPPLEMENTAL INFORMATION

Supplemental information can be found online at https://doi.org/10.1016/j.isci.2022.103758.

ACKNOWLEDGMENTS

The authors thank the staff of ANICAN (Cancer Research Center of Lyon) staff for the maintenance of the mouse strains and Christophe Vanbelle for the helpful assistance with the confocal microscopy experiments. We also thank Brigitte Manship for proofreading the manuscript. This study was supported by grants from La Ligue Contre le Cancer (A.H.), Bristol Meyers Squibb Foundation (A.H.), Inserm Transfert (A.H.), Sanofi iAward (A.H), INCaAAP 2019 (A.H.), and Fondation de France (A.H. and P.G.), WZC was supported by a Chinese Scholarship Council (CSC) Fellowship.

AUTHOR CONTRIBUTIONS

S.B performed the experiments and analyzed the data. Z.W., P.G., and K.T. performed the experiments. P.M. and J.C. performed the AFM experiments and analysis. A.H. designed the experiments, analyzed the data, and wrote the manuscript. A.H. is the guarantor of this work and thus had full access to all the data obtained in the study and takes responsibility for the integrity of the data and the accuracy of the data analysis.

DECLARATION OF INTERESTS

The authors have no conflicts of interest to disclose.

Received: July 20, 2021
Revised: October 27, 2021
Accepted: January 7, 2022
Published: February 18, 2022

REFERENCES

Bae, J.S., Lee, S.H., Kim, J.E., Choi, J.Y., Park, R.W., Yong Park, J., Park, H.S., Sohn, Y.S., Lee, D.S., Bae Lee, E., and Kim, I.S. (2002). Betaig-h3 supports keratinocyte adhesion, migration, and proliferation through alpha3beta1 integrin. Biochem.biophysicalRes.Commun. *294*, 940–948.

Bayne, L.J., Beatty, G.L., Jhala, N., Clark, C.E., Rhim, A.D., Stanger, B.Z., and Vonderheide, R.H. (2012). Tumor-derived granulocyte-macrophage colony-stimulating factor regulates myeloid inflammation and T cell immunity in pancreatic cancer. Cancer cell *21*, 822–835.

Diskin, B., Adam, S., Cassini, M.F., Sanchez, G., Liria, M., Aykut, B., Buttar, C., Li, E., Sundberg, B., Salas, R.D., et al. (2020). PD-L1 engagement on T cells promotes self-tolerance and suppression of neighboring macrophages and effector T cells in cancer. Nat. Immunol. *21*, 442–454.

Galon, J., Costes, A., Sanchez-Cabo, F., Kirilovsky, A., Mlecnik, B., Lagorce-Pages, C., Tosolini, M., Camus, M., Berger, A., Wind, P., et al. (2006). Type, density, and location of immune cells within human colorectal tumors predict clinical outcome. Science *313*, 1960–1964.

Goehrig, D., Nigri, J., Samain, R., Wu, Z., Cappello, P., Gabiane, G., Zhang, X., Zhao, Y., Kim, I.S., Chanal, M., et al. (2019). Stromal protein betaig-h3 reprogrammes tumour microenvironment in pancreatic cancer. Gut *68*, 693–707.

Hashimoto, K., Noshiro, M., Ohno, S., Kawamoto, T., Satakeda, H., Akagawa, Y., Nakashima, K., Okimura, A., Ishida, H., Okamoto, T., et al. (1997). Characterization of a cartilage-derived 66-kDa protein (RGD-CAP/beta ig-h3) that binds to collagen. Biochim.Biophys. Acta *1355*, 303–314.

Hingorani, S.R., Petricoin, E.F., Maitra, A., Rajapakse, V., King, C., Jacobetz, M.A., Ross, S., Conrads, T.P., Veenstra, T.D., Hitt, B.A., et al. (2003). Preinvasive and invasive ductal pancreatic cancer and its early detection in the mouse. Cancer cell *4*, 437–450.

Hu, H., Hang, J.J., Han, T., Zhuo, M., Jiao, F., and Wang, L.W. (2016). The M2 phenotype of tumor-associated macrophages in the stroma confers a poor prognosis in pancreatic cancer. Tumour Biol. *37*, 8657–8664.

Kuczek, D.E., Larsen, A.M.H., Thorseth, M.L., Carretta, M., Kalvisa, A., Siersbaek, M.S., Simoes, A.M.C., Roslind, A., Engelholm, L.H., Noessner, E., et al. (2019). Collagen density regulates the activity of tumor-infiltrating T cells. J. Immunother.Cancer *7*, 68.

Laklai, H., Miroshnikova, Y.A., Pickup, M.W., Collisson, E.A., Kim, G.E., Barrett, A.S., Hill, R.C., Lakins, J.N., Schlaepfer, D.D., Mouw, J.K., et al. (2016). Genotype tunes pancreatic ductal adenocarcinoma tissue tension to induce matricellular fibrosis and tumor progression. Nat.Med. *22*, 497–505.

Larsen, A.M.H., Kuczek, D.E., Kalvisa, A., Siersbaek, M.S., Thorseth, M.L., Johansen, A.Z., Carretta, M., Grontved, L., Vang, O., and Madsen, D.H. (2020). Collagen density modulates the immunosuppressive functions of macrophages. J. Immunol. *205*, 1461–1472.

Liu, C.Y., Xu, J.Y., Shi, X.Y., Huang, W., Ruan, T.Y., Xie, P., and Ding, J.L. (2013). M2-polarized tumor-associated macrophages promoted epithelial-mesenchymal transition in pancreatic cancer cells, partially through TLR4/IL-10 signaling pathway. Lab.Invest. *93*, 844–854.

Mantovani, A., Sica, A., Sozzani, S., Allavena, P., Vecchi, A., and Locati, M. (2004). The chemokine system in diverse forms of macrophage activation and polarization. Trends Immunol. *25*, 677–686.

Milani, P., Mirabet, V., Cellier, C., Rozier, F., Hamant, O., Das, P., and Boudaoud, A. (2014). Matching patterns of geneexpression to mechanical stiffness at cell resolution through quantitative tandem epifluorescence and nanoindentation. Plant Physiol. *165*, 1399–1408.

Patry, M., Teinturier, R., Goehrig, D., Zetu, C., Ripoche, D., Kim, I.S., Bertolino, P., and Hennino, A. (2015). betaig-h3represses T-cell activation in type 1 diabetes. Diabetes *64*, 4212–4219.

Ruiz-Valdepenas, L., Martinez-Orgado, J.A., Benito, C., Millan, A., Tolon, R.M., and Romero, J. (2011). Cannabidiol reduces lipopolysaccharide-induced vascular changes and inflammation in the mouse brain: an intravital microscopy study. J. Neuroinflammation *8*, 5.

Schneider, C.A., Rasband, W.S., and Eliceiri, K.W. (2012). NIH Image to ImageJ: 25 years of image analysis. Nat. Methods *9*, 671–675.

Skonier, J., Bennett, K., Rothwell, V., Kosowski, S., Plowman, G., Wallace, P., Edelhoff, S., Disteche, C., Neubauer, M., Marquardt, H., et al. (1994). Beta ig-h3: a transforming growth factor-beta-responsive gene encoding a secreted protein that inhibits cell attachment in vitro and suppresses the growth of CHO cells in nude mice. DNA Cell Biol *13*, 571–584.

Skonier, J., Neubauer, M., Madisen, L., Bennett, K., Plowman, G.D., and Purchio, A.F. (1992). cDNA cloning and sequence analysis of beta ig-h3, a novel gene induced in a human adenocarcinoma cell line after treatment with transforming growth factor-beta. DNA Cell Biol. *11*, 511–522.

Zhu, Y., Herndon, J.M., Sojka, D.K., Kim, K.W., Knolhoff, B.L., Zuo, C., Cullinan, D.R., Luo, J., Bearden, A.R., Lavine, K.J., et al. (2017). Tissue-resident macrophages in pancreatic ductal adenocarcinoma originate from embryonic hematopoiesis and promote tumor progression. Immunity *47*, 597.

STAR★METHODS

KEY RESOURCES TABLE

REAGENT or RESOURCE	SOURCE	IDENTIFIER
Antibodies		
Rabbit polyclonal anti-βig-h3	Sigma-Aldrich	Cat# HPA008612, RRID:AB_1857970
Mouse monoclonal anti-collagen I (clone 3G3)	Abcam	Cat# ab88147, RRID:AB_2081873
Rat monoclonal to F4/80 (clone CI:A3-1)	Abcam	Cat#ab6640 RRID:AB_1140040
Mouse monoclonal anti-CD206 (Mannose receptor) (clone 15-2)	Abcam	Cat# ab8918, RRID:AB_306860
Donkey polyclonal Anti-Rabbit IgG (H + L), Alexa Fluor 647-conjugated	Invitrogen/Thermo Fisher Scientific	Cat# A-31573, RRID:AB_2536183
Donkey polyclonal anti-Mouse IgG (H + L), Alexa Fluor 555-conjugated	Invitrogen/Thermo Fisher Scientific	Cat# A-31570, RRID:AB_2536180
Donkey polyclonal anti-Rat IgG (H + L), Cy3-conjugated	Jackson Immunoresearch	Cat#712-166-150 RRID:AB_2340668
Phalloidin, Alexa Fluor 488-conjugated	Cell Signaling Technology	Cat#8878S RRID:AB_2315147
Rabbit monoclonal anti-Phospho-FAK (Tyr397) (clone 31H5L17)	Invitrogen/Thermo Fisher Scientific	Cat# 700,255, RRID:AB_2532307
Rabbit polyclonal anti-FAK	Cell signaling Technology	Cat#3285 RRID: AB 2269034
Anti-tubulin	GeneTex	Cat#GTX628802
anti-pERK	Cell Signaling	Cat#4695
Donkey polyclonal Anti-Rabbit IgG (H + L), HRP-conjugated	Jackson ImmunoResearch Labs	Cat# 711-035-152, RRID:AB_10015282
Rat monoclonal anti-F4/80 (clone BM8), PE-Cy7-conjugated	Biolegend	Cat# 123114, RRID:AB_893478
Rat monoclonal anti-F4/80 (clone BM8), PerCP-Cy5.5-conjugated	Biolegend	Cat# 123128, RRID:AB_893484
Rat monoclonal anti-MHC Clas II (I-A/I-E) (clone M5/114.15.2), PE-Cy7-conjugated	eBioscience/Thermo Fisher Scientific	Cat# 12-5321-81, RRID:AB_465927
Rat monoclonal anti-CD206 (clone C068C2), Brilliant Violet 650-conjugated	Biolegend	Cat# 141723, RRID:AB_2562445
Rat monoclonal anti-CD86 (clone GL-1), APC-Cy7-conjugated	Biolegend	Cat# 105030, RRID:AB_2244452
Armenian hamster monoclonal anti-CD80 (clone 16-10A1), Brilliant Violet 605-conjugated	Biolegend	Cat# 104729, RRID:AB_11126141
Rat monoclonal anti-CD115 (CSF-1R) (clone AFS98), APC-Cy7-conjugated	Biolegend	Cat# 135511, RRID:AB_11218605
Rat monoclonal anti-iNOS (clone CXNFT), PE-conjugated	Life Technlogies/Thermo Fisher Scientific	Cat# 12-5920-82, RRID:AB_2572642
Sheep polyclonal anti-Arginase 1/ARG1, APC-conjugated	R&D Systems	Cat# IC5868A, RRID:AB_2810265
Mouse monoclonal anti-LAP (TGF-beta-a) (clone TW7-16B4), Brilliant Violet 421-conjugated	Biolegend	Cat# 141408, RRID:AB_2650898
Human/mouse monoclonal anti-Granzyme B (clone GB11), Alexa Fluor 647 conjugated	Biolegend	Cat#515406 RRID:AB 2566333

(*Continued on next page*)

Continued

REAGENT or RESOURCE	SOURCE	IDENTIFIER
Rat monoclonal anti-IFN gamma (clone XMG1.2), Brillant Violet 650-conjugated	Biolegend	Cat#505831 RRID:AB_11142685
Rat monoclonal anti-TNF-alpha (clone MP6-XT22), Brilliant Violet 605-conjugated	Biolegend	Cat# 506329, RRID:AB_11123912
Hamster anti-mouse CD69 (clone H1.2F3), PerCP-Cy5.5-conjugated	BD Bioscences	Cat#551113 RRID:AB_394051
Rat anti-human/mouse CD44 (clone IM7), Alexa Fluor 700 conjugated	Biolegend	Cat#103025 RRID:AB_493712
Rat anti-mouse CD163 (clone TNKUPJ), PE conjugated	eBioscience/Thermo Fisher Scientific	Cat#12-1631-82 RRID:AB_2716924
anti-βig-h3 18B3	(Goehrig et al., 2019)	(Goehrig et al., 2019)
IgG1 control Ab	BioXcell, USA	BE0083
Chemicals, peptides, and recombinant proteins		
Collagen I	Gibco/Thermo Fisher Scientific	Cat#A10483-01
Phosphate-buffered saline (PBS) 10x	Gibco/Thermo Fisher Scientific	Cat#14190-144
Phosphate-buffered saline (PBS) 1x	Gibco/Thermo Fisher Scientific	Cat#14190-144
Human recombinant βig-h3 protein	Bio-Techne/RD	Cat#3409-BG
Dulbecco's Modified Eagle Medium (DMEM)	Gibco/Thermo Fisher Scientific	Cat#61965059
Fetal calf serum (FCS)	Eurobio	Cat#CVFSVF00-01
Penicillin-Streptomycin (P/S)	Gibco/Thermo Fisher Scientific	Cat#15140-122
Collagenase P	Roche/Sigma-Aldrich	Cat#11213865001
Triton X-100	Sigma-Aldrich	Cat#T8787
16% Formaldehyde solution (PFA)	Termo Fisher	Cat#28908
Antigen Unmasking Solution, Citrate-Based	Vector/Eurobio	Cat#H-3300
Antibody diluent Reagent	Life Techno/Thermo Fisher	Cat#003218
Vectashield mounting medium with DAPI	Vector/Eurobio	Cat#H-1200
NuPAGE 4-12% Bis-Tris polyacrylamide gel	Invitrogen/Thermo fischer	Cat#NP0335BOX
Immun-Blot PVDF membrane	Biorad	Cat#1620177
Tris buffered saline (TBS)	Euromedex	Cat#ET220
Tween 20	VWR	Cat#28829.296
Bovine serum albumin (BSA)	Sigma	Cat#A2153-100G
RIPA buffer	Pierce/Thermo Fisher	Cat#89900
Protease complete EDTA-free	Roche/Sigma-Aldrich	Cat#04 693 159 001
Phosphatase phoSTOP	Roche/Sigma-Aldrich	Cat#04 906 837 001
Brefeldin A solution	Biolegend	Cat#420601
Dynabeads™ Mouse T-Activator CD3/CD28 for T-Cell Expansion and Activation	Gibco/Thermo Fisher Scientific	Cat#11452D
Corning® Matrigel® Basement Membrane Matrix High Concentration	Corning	Cat#354248
CD8a (Ly-2) microbeads mouse	Miltenyi Biotec	Cat#130-117-044
FAK Inhibitor 14	Sigma-Aldrich	Cat#SML0837
Critical commercial assays		
ECL chemiluminescence kit	Pierce Chemical/Thermo Fisher Scientific	Cat#32106
Fixation/permeabilisation kit	BD	Cat#554714
CellTrace™ Violet Cell Proliferation Kit	Invitrogen/Thermo Fisher Scientific	Cat#C34557
CellTrace™ CFSE Cell Proliferation Kit	Invitrogen/Thermo Fisher Scientific	Cat#C34554

(*Continued on next page*)

Continued

REAGENT or RESOURCE	SOURCE	IDENTIFIER
Experimental models: Cell lines		
L929 cells	ATCC CCL-1	ATCC CCL-1
Tumoral cells Epi	(Goehrig et al., 2019)	(Goehrig et al., 2019)
Experimental models: Organisms/strains		
C57BL/6 (WT) mice	Envigo	C57bL/6JOlaHsd
$P48^{+/Cre}$;$Kras^{G12D}$ (KC) mice	(Hingorani et al., 2003)	Hingorani et al. (2003)
Software and algorithms		
ImageJ	Schneider et al., 2012(Schneider et al., 2012)	https://imagej.net
BD FACSDiva™ Software	BD Biosciences	https://www.bdbiosciences.com
FlowJo	Becton, Dickinson and Company, 2019	https://www.flowjo.com
Python 3.0 processing	BIOMECA	https://www.bio-meca.com
Nanoscope software 9.1.R.3	BIOMECA	https://www.bio-meca.com

RESOURCE AVAILABILITY

Lead contact

Further information and requests for resources and reagents should be directed to and will be fulfilled by the lead contact Ana Hennino (ana.hennino@inserm.fr).

Materials availability

This study did not generate new unique reagents.

Data availability

- All data reported in this paper will be shared by the lead contact upon request.
- This paper does not report original code.
- Any additional information required to reanalyze the data reported in this paper is available from the lead contact upon request.

METHOD DETAILS

Mice

C57BL/6 mice (WT) were obtained from Envigo (Indianapolis/Indiana/USA). KC mice, KIC mice and Rag2-KO mice were bred in house (males and females). All mice were kept under specific pathogen-free conditions at the Animale en Cancérologie (AniCan) platform at the Cancer Research Center of Lyon (CRCL). All animal procedures and experiments were performed in compliance with the ethical guidelines of the CRCL Animal Care and Use Committee, with approval of the Experimental Animal Ethics Committee of the Rhône-Alpes region (CECCAPP) (CECCAPP_CLB_2019_002).

Generation of collagen matrices

Collagen I matrix was prepared by carefully mixing 800 µL of collagen I (Gibco; Amarillo/TX/USA) with 7,000 µL of 1x PBS (Gibco; Amarillo/TX/USA), 100 µL of 10x PBS and 100 µL of NaOH 0.1M. 8 mL of collagen I matrix at 300 µg/mL was added on a 10 cm^2 Petri dish and allowed to solidify at 37°C for at least 1 h. For βig-h3 structured collagen, rβig-h3 (Bio-Techne; Minneapolis/Minnesota/USA) was added to the collagen I matrix mix at a final concentration of 2.5 µg/mLprior to the solidification.

BMMC generation and education

In order to generate bone marrow-derived monocytes, bone marrow cell suspensions were isolated by flushing femurs and tibias of 8-12 week-old C57BL/6 mice with Dulbecco's Modified Eagle Medium (DMEM) (Gibco; Amarillo/TX/USA) containing 10% of foetal calf serum (FCS) (Eurobio; Evry-France) and 1% penicilin/streptomycin (P/S) (10,000 U/mL penicillin and 10 mg/mL of streptomycine; Gibco; Amarillo/TX/USA) (DMEM-c). Cell aggregates were dislodged by passing the suspension through a 100µm

cell strainer. Lysis of red blood cells was performed with in house-made ammonium-chloride-potassium (AKC) lysis buffer. 10 millions cells obtained were resuspended in 10 mL of DMEM-c supplemented with 20% of supernatant from L292 cells containing M-CSF plated on a 10 cm^2 tissue culture dish, and incubated for 6 days at 37°C, CO_2 5%. Every other day, 10 mL of medium was removed and fresh DMEM-c supplemented with 20% M-CSF was added to the cells. Cells were harvested at day 7. For BMMC education, 10^7 cells were seeded onto 10 cm^2 tissue culture dish coated with collagen or collagen+βig-h3 matrices previously described for 48 hat 37°C.

KIC tumor cell line

The isolation and culture of KIC pancreatic tumor cells from KIC mice, which were generated on a C57BL/6 background, was performed by modifying a previously published protocol (Bayne et al., 2012; Goehrig et al., 2019). Briefly, the excised pancreas of a 2.5-month-old KIC mouse was minced into small fragments and then incubated in 1x PBS containing collagenase V (1 mg/mL; Roche; Basel/Switzerland) at 37°C for 20 minutes. The digested tissue was homogenized by passage through a 100 μm cell strainer and the obtained cells were plated into 6-well plates with serum-free DMEM. After 2 weeks, the medium was changed to DMEM-c. After three to six passages, the cells were infected with lentiviral vector expressing H2B GFP (Addgene no 25999).

Atomic force microscopy measurements and collagen fibrils analysis

AFM measurements were performed in the BIOMECA laboratory (ENS, Lyon) with a Resolve Bioscope (Bruker Nano Surface, Santa Barbara, CA) mounted on an inverted optical DMI8 (Leica). AFM measurements were performed using a conical tip located on a flexible cantilever with a 0.35 N/m spring constant (DNP-10A, Bruker AFM probes). Before each experiment, the deflexional sensitivity of the cantilever was calibrated against a sapphire wafer and spring constant was measured using the thermal tune method. All experiments were conducted on sample sections immersed in PBS (Capricorn-scientific) at room temperature and the standard cantilever holder for operation in liquid was used. Data acquisition was made with the Nanoscope software, 9.1.R.3 version, on AFM QNM mode (Quantitative Nanomechanical Mapping), in fluid condition. Experiments consisted in acquiring topographic images (5 μm × 5 μm, 20nN of force, 8μm ramp size and 1.0 Hz ramp rate). Collagen fibrils thickness was analyzed using a BIOMECA's analysis script on PYTHON 3.0 processing. The AFM images were converted to a binary black and white image and analyzed by a skeletonized approach to extract collagen fibril thickness. Using the stiffness constant of the lever, the deflection indicates the resistance of the sample. Our protocol (Milani et al., 2014) allows us to measure the local stiffness of the matrices in a minimally invasive manner, by deforming the samples down to a depth of 100 nm. In order to investigate the stiffness patterns at high resolution we used the quantitative nanomechanical mapping and the force volume protocols (Bruker). In these protocols, the AFM probe oscillates at low frequency while horizontally scanning the sample and a force curve in generated each time the probe enters in contact with the sample. The elastic modulus of the sample, which reflects the stiffness, is then extracted from each curve applying the Sneddon (Hertz) model, yielding two-dimensional stiffness maps, where each pixel represents one force curve.

Immunofluorescence staining

Paraffin embedded mouse tissue was sectioned at a thickness of 4 μm thick on a Microtome (Leica; Wetzlar/Germany). The sections were deparaffinized and rehydrated before antigen unmasking was performed using unmasking solution Vector H 3300 (Eurobio; Evry-France). The sections were saturated with antibody (Ab) diluent (Dako/Agilent; Santa Clara/CA/USA) for 30 min and then incubated overnight at 4 °C with primary Abs that were appropriately diluted in Ab diluent. The next day, the sections were incubated with specific secondary Abs that were diluted in Ab diluent. Finally, the sections were mounted in Vectashield mounting medium containing DAPI (Eurobio; Evry-France) for nuclear counterstaining.

For phalloidin staining 4 × 10^5 BMMC were cultured in P12 plates equipped with circular cover slips coated with collagen or collagen + rβig-h3 for 24 h. The cover slips were recovered and washed in PBS. Attached cells were fixed with PFA 4% for 5 min and permeabilized in PBS 0.2% Triton for 6minat RT. Cells were stained with phalloidin overnight at 4 °C and then mounted in Vectashield mounting medium containing DAPI (Eurobio; Evry-France) for nuclear counterstaining.

Confocal microscopy

All samples were visualized under an LSM 880 inversed confocal microscope (Zeiss/Provenance). Series of images were collected and processed using ImageJ software. For the analysis of BMMC processes 10 regions of interest (ROI) were analyzed.

Western blot

Educated BMMCs were collected by scratching in 10 mL of PBS. After centrifugation, the proteins were isolated using RIPA buffer supplemented with protease and phosphatase inhibitors. 20μL of the obtained lysate were separated by NUPAGE 4-12% Bis-Tris Gel electrophoresis (SDS- PAGE) (Gibco; Amarillo/TX/USA) and transferred to a Immune-Blot PVDF membrane (Biorad; Hercules/Californie/USAs). After transfer, the immune-blots were blocked by incubating with 5% BSA in Tris buffered saline (TBS) (Euromedex; Souffelweyersheim/France) containing 0.05% Tween 20 (VWR; Radnor/Pennsylvanie/USA). The blots were then probed overnight with appropriately diluted primary Abs. After washing in TBS-Tween 0.05%, the membranes were revealed with secondary antibodies for 1 hour at room temperature. After washing, the blots were developed using the ECL chemiluminescence method according to the manufacturer's protocol (Pierce Chemical; Waltham/MA/USA).

The following antibodies were used to detect their corresponding substrates: anti-pFAK from Invitrogen, FAK from Cell Signalling, pERK from Cell Signaling and anti-tubulin obtained from GeneTex. Either HRP-conjugated anti-rabbit or anti-mouse Abs (Jackson Immunoresearch; Ely/United Kingdom) were used for primary antibody binding.

FACS analysis

Educated BMMCs were collected by scratching into 10 mL of PBS and centrifuged. In case of tumor implantation, the tumor grafts were excised, weighed and measured. The tumor grafts were then digested in PBS (Gibco; Amarillo/TX/USA) supplemented with collagenase (1 mg/mL; Roche; Basel/Switzerland) for 20 minat 37°C. The digested tissue was homogenized by passage through a 100μm cell strainer. Single cell suspensions from BMMCs or tumor grafts were stained with fluorescently labelled antibodies for 20 minat 4°C. For cytokine analysis single cell suspensions were incubated with Brefeldin A (Biolegend; San Diego/CA/USA) for 2h at 37°C prior to surface staining in order to retain intracellular proteins. After surface staining, cells were fixed and permeabilized using the Fixation/Permeabilization kit according to the manufacturer's protocol (BD; New Jersey/USA) and intracellular staining was performed for 30 minat 4°C. Fluorescently labelled cells were acquired on a BD Fortessa Flow Cytometer (BD; Franklin Lakes/NJ/USA) and analyzed using either BD FACS Diva software V.5.0.1 (BD; Franklin Lakes/NJ/USA) or FlowJo (Tree Star/BD; Franklin Lakes/NJ/USA).

The following monoclonal Abs were used in flow cytometry: anti-F4/80 Pe-Cy7 (clone BM8-Biolegend, 123114) or PerCP Cy5.5 (clone BM8-Biolegend, 123128), anti-MHCII PE (clone M5/114.15.2- eBioscience, 12-5321-81), anti-CD206 BV650 (clone C068C2-Biolegend, 141723), anti-CD86 BV605 (clone GL-1- Biolegend, 105029), anti-CD80 APC-Cy7 (clone 16-10A1-Biolegend, 104729), anti-CSFRI AF488 (clone AFS98- Biolegend, 135511), anti-INOS PE (clone CXNFT, Life Techno, 12-5920-82), anti-Arginase1 APC (RD, IC5868A), anti-TGF-β B421 (clone TW7-16B4-Biolegend, 141408) and anti-TNFα BV605 (clone MP6-XT22-Biolegend, 506329).

T cell activation assay

$CD8^+$T cells were purified from the spleens and lymph nodes of female C57BL/6 mice by column-based magnetic activated cells sorting (MACS) according to the manufacturer's protocol (Miltenyi Biotec; Bergisch Gladbach/Germany). Purified $CD8^+$T cells were thenlabelled with 5μM CSFE at 37 °C for 20min in PBS according to the manufacturer's protocol (Invitrogen; Amarillo/TX/USA). Following, CFSE-labelled $CD8^+$T cells were then cultured for two days in the presence of BMMCs respecting the T cell:BMMC ratios of 4:1, 2:1 and 1:1. Dynabeads^{TM} Mouse T-Activator CD3/CD28 for T-cell expansion and Activation (Gibco; Amarillo/TX/USA) were added to the co-culture respecting at a T cell:bead ratio of 1:1. Proliferation of $CD8^+$T cells was evaluated at the end of the culture period by analysing CFSE dilution using flow cytometry.

Short term tumor implantation assay

BMMCs were generated *in vitro* and educated for 48 hat 37 °C on collagen matrices structured in the presence or absence of rhβig-h3 as described above. BMMCs were then harvested using trypsin action, and

labelled with 5μM Cell Trace Violet at 37 °C for 20min according to the manufacturer's protocol (Invitrogen; Amarillo/TX/USA).

Tumor cells line were generated in the lab like as described previously. The cells were routinely cultured in DMEM-c and recovered by trypsinization.

Next, 1 × 10^6 cells BMMCs and 5×10^5 tumor cells were resuspended in a Matrigel 1:1 mix (Matrigel Matrix HC Cat 354248 Corning; Glendale/Arizona/USA) and subcutaneously injected as plugs into the flank of C57BL/6 mice.

For some experiments, 5×10^5 cells tumor cells were resuspended in a collagen I mix (300 μg/mL) with or without rhβig-h3 (2.5 μg/mL) and subcutaneously injected as plugs into the flank of Rag2KO mice. In both experimental setups, the mice were monitored on a daily basis. Five days after the engraftments, the mice were sacrificed and the tumor plugs were recovered.

Alternatively KIC cells (5×10^5) were subcutaneously injected into C57BL/6 mice. Ten days later, mice were treated twice a week for two weeks with an anti-βig-h3 depleting Ab (6 μg) or isotype control Ab (6 μg, Bioxcell). Mice were then monitored for 14 days and then sacrificed. The tumor grafts were then weighed, measured and processed for flow cytometric analysis.

QUANTIFICATION AND STATISTICAL ANALYSIS

The p-values were calculated using Student's t-test with GraphPad Prism as indicated in the figure legends: *$p < 0.05$, **$p < 0.01$, ***$p < 0.001$ and ****$p < 0.0001$. One-way ANOVA with Tukey's post hoc test was used for multiple comparisons.